Geomorphological control on boulder transport and coastal erosion before, during and after an extreme extra-tropical cyclone

Larissa A. Naylor,[1]* Wayne J. Stephenson,[2] Helen C. M. Smith,[3] Oliver Way,[4] James Mendelssohn[5] and Andrew Cowley[3]
[1] School of Geographical and Earth Sciences, University of Glasgow, Glasgow, UK
[2] Department of Geography, University of Otago, Dunedin, New Zealand
[3] University of Exeter, Penryn, UK
[4] Arcadis Consulting (UK), Exeter, UK
[5] Emeritus, Atlantic United World College, St Donat's, UK

*Correspondence to: Larissa A. Naylor, School of Geographical and Earth Sciences, University of Glasgow, Glasgow, G12 8QQ, UK. E-mail: larissa.naylor@glasgow.ac.uk

Earth Surface Processes and Landforms

ABSTRACT: Extreme wave events in coastal zones are principal drivers of geomorphic change. Evidence of boulder entrainment and erosional impact during storms is increasing. However, there is currently poor time coupling between pre- and post-storm measurements of coastal boulder deposits. Importantly there are no data reporting shore platform erosion, boulder entrainment and/or boulder transport during storm events – rock coast dynamics during storm events are currently unexplored. Here, we use high-resolution (daily) field data to measure and characterize coastal boulder transport before, during and after the extreme Northeast Atlantic extra-tropical cyclone Johanna in March 2008. Forty-eight limestone fine-medium boulders ($n = 46$) and coarse cobbles ($n = 2$) were tracked daily over a 0.1 km^2 intertidal area during this multi-day storm. Boulders were repeatedly entrained, transported and deposited, and in some cases broken down ($n = 1$) or quarried ($n = 3$), during the most intense days of the storm. Eighty-one percent ($n = 39$) of boulders were located at both the start and end of the storm. Of these, 92% were entrained where entrainment patterns were closely aligned to wave parameters. These data firmly demonstrate rock coasts are dynamic and vulnerable under storm conditions. No statistically significant relationship was found between boulder size (mass) and net transport distance. Graphical analyses suggest that boulder size limits the maximum longshore transport distance but that for the majority of boulders lying under this threshold, other factors influence transport distance. Paired analysis of 20 similar sized and shaped boulders in different morphogenic zones demonstrates that geomorphological control affects entrainment and transport distance – where net transport distances were up to 39 times less where geomorphological control was greatest. These results have important implications for understanding and for accurately measuring and modelling boulder entrainment and transport. Coastal managers require these data for assessing erosion risk. © 2016 The Authors. Earth Surface Processes and Landforms published by John Wiley & Sons Ltd.

KEYWORDS: extra-tropical cyclone; boulder transport; geomorphological control; coastal erosion; storm

Introduction

There is mounting (but still limited) evidence for storm induced boulder movement in a range of geomorphological settings (Paris *et al.*, 2011). Recent research has documented storm-driven, bi-monthly to century timescale changes in coastal boulder deposits in subtidal (Mastronuzzi and Sanso, 2004), intertidal (Chen *et al.*, 2011; Knight and Burningham, 2011; Peréz-Alberti and Trenhaile, 2015), supratidal (Noormets *et al.*, 2004; Goto *et al.*, 2013) and cliff-top (Hansom *et al.*, 2008; Fichaut and Suanez, 2011) settings. These typically report movement of boulders months to years before and after a storm and reflect poor time-coupling between field observations and actual storm events. Data before, during and after specific storm-events are currently lacking and are critical in

understanding and predicting boulder responses to past, present or future storms (Noormets *et al.*, 2004; Imamura *et al.*, 2008; Goto *et al.*, 2011). Such data may also help differentiate sedimentary signatures of palaeo boulder deposits (Lorang, 2011).

The data presented here represents the first known storm-event specific dataset on coastal boulder transport globally. We show that high-resolution, daily data from contemporary storms can add useful insight into the factors controlling boulder morphodynamics. In addition to advancing our understanding of current process dynamics, these data can aid sedimentological studies of tsunamis and storms by providing evidence of how extreme storms alter rocky coasts and how rock coast geomorphology meditates these processes. These data can help shed light on the critical factors controlling entrainment and sediment transport under storm conditions, potentially leading

to improved equations and palaeo-environmental reconstructions. Accurate palaeo-environmental reconstructions are an important means of calculating recurrences intervals of extreme storm and flood events that extend beyond relatively short experimental records (e.g. Foulds and Macklin, 2016). Importantly, this high-resolution, daily data before, during and immediately following a storm allows us to answer key questions posed by sedimentologists and geomorphologists operating over a range of timescales (i.e. hours to millennium). Is boulder size a significant factor influencing entrainment and transport? Which factors, in addition to boulder size, are important controls on entrainment and transport distance? Accurate parameterization of these controls is crucial for improving the accuracy of models and palaeo-reconstructions of past extreme events.

These data are particularly important as recent climate models suggest that Northern Hemisphere extra-tropical cyclones will become more intense in the late twenty-first century (Mitzuta *et al.*, 2011), and that the British Isles will experience more frequent winter storms (McDonald, 2011). The recent intense storms in the British Isles during the winter of 2013 to 2014 led to dramatic rock coast and gravel beach erosion (Earlie *et al.*, 2015; Masselink *et al.*, 2016); these have been partly attributed to the changing climate (Met Office, 2014).

Study Site and Extra-Tropical Cyclone Johanna

The study site is located in the Bristol Channel (51.2350 N 3.3230 W), a macrotidal (i.e. 9–11 m tidal range) estuary exposed to large storm waves (e.g. average significant wave height of 2 to 2.5 m and storm waves exceeding 5.5 m; Figure 1A). The entire shore platform and cliff base are inundated during each tidal cycle and are thus affected by waves (swash and backwash conditions) and subaerial erosion processes (Naylor *et al.*, 2012). The site is composed of wide (~ 300 m), seaward dipping (3° dip, 185° dip direction) cliff backed Blue Lias limestone
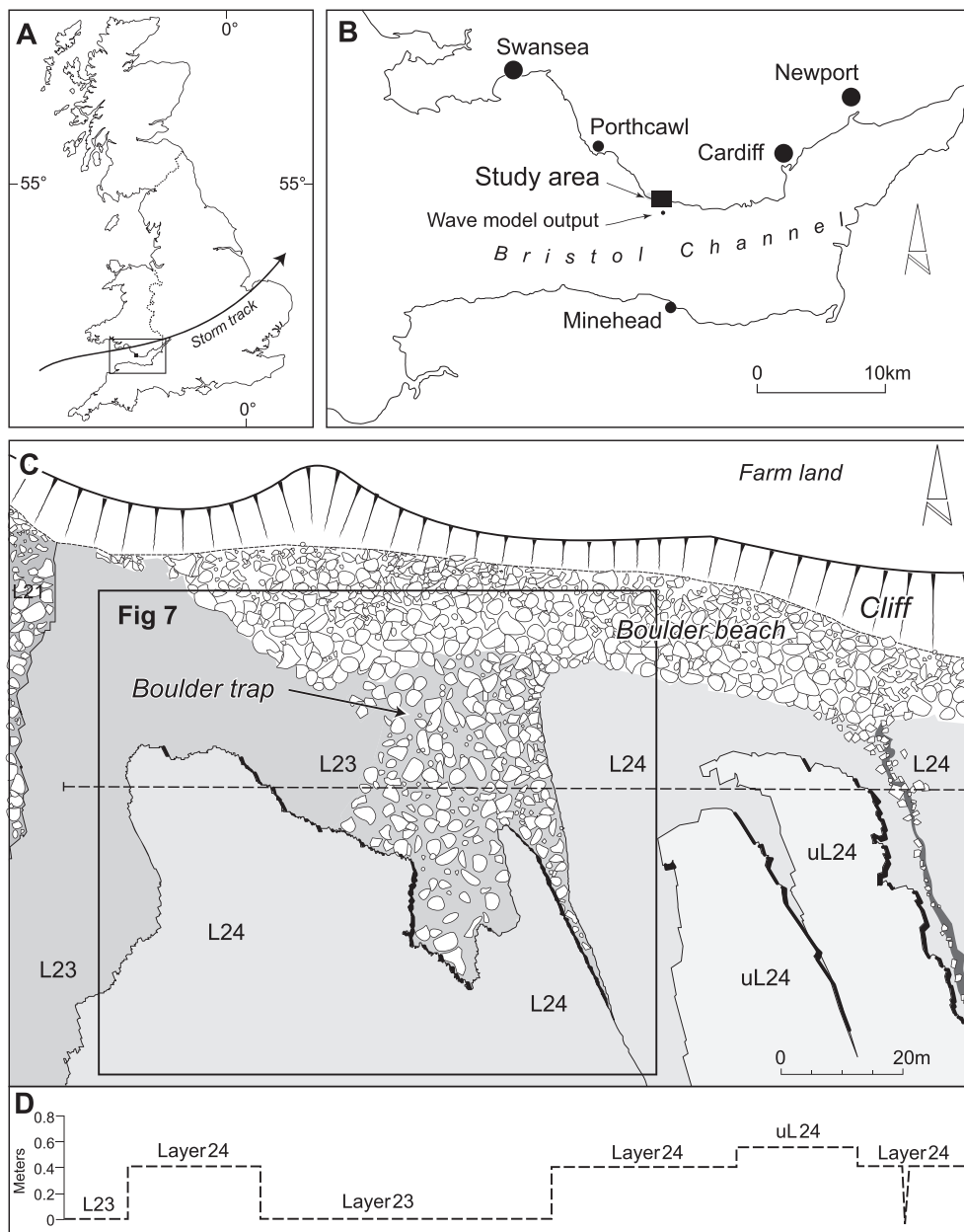
Figure 1. (A) Study site location denoting the sampling area, the wave model output location and wave model calibration point. The curved arrow in the inset map denotes the approximate storm pathway (after Cariolet *et al.*, 2010). (B) Map showing the three morphogenic zones across the bed layer 24 portion of the study area, along with a cross-shore profile illustrating the change in vertical elevation across the sampling area. (C) Depicts the morphogenic context of the L24 study area, showing the spatial relationships between different morphogenic zones. (D) Cross-section of changes in platform elevation across the L24 study area (see dashed line in (C) for the location of this profile).

(effective porosity =0.9877–0.9905 and compressive strength =59 kg/cm^2) intertidal shore platforms (Naylor, 2001). The platforms have three distinctive morphogenic zones (platform, boulder trap and boulder beach, after Paris *et al.* 2011; Figures 1B and 2; Table I).

Between 10 and 12 March 2008 extra-tropical cyclone Johanna tracked across northwest Europe creating intense low pressures, gale-force winds and extreme waves (i.e. significant wave height (H_s) over 17 m at K2 buoy (51.000 N 13.301 W) (Turton and Fenna, 2008). The extra-tropical cyclone Johanna coincided with a 12 m spring tide and at the nearest wave buoy (located at Minehead, Devon, Figure 1A) the highest recorded wave at the buoy was 5.96 m H_{max} at 23:00 on 10 March. It led to flooding and storm damage across the British Isles and France (e.g. Cariolet *et al.*, 2010).

We collected daily data (pre-storm, during and post-storm) quantifying individual intertidal boulder detachments (i.e. shore platform erosion), entrainment, transport and breakdown in south Wales, UK (Figure 1A). Pre-storm data were collected on 9 March, storm data between the 10 and 12 March and post-storm data on 13 March 2008. This represents the highest resolution dataset known globally and critically, has data during the storm as well as immediately before and after the storm. We

also contextualize these individual boulders by illustrating how dynamic the wider population of boulders were during the storm event. Thus, our boulder sample provides quantitative evidence of individual boulders within the context of a dynamic, shifting boulder population.

Methods

Wave modelling

The wave heights at the survey site during the March storm were modelled using the SWAN (Simulating Waves Nearshore) wave model (Booji *et al.*, 1999). Boundary wave conditions were provided by output from the British Meteorological Office (BMO) second generation UK Waters wave model, with wind data from the BMO Unified Model (Bidlot and Holt, 1999) and tidal heights taken from predictions for Porthcawl, 14 km northwest of the survey site. Three hourly offshore wave states were transformed to predict significant wave height, H_s, mean wave period, T_z, and direction. The actual model output point is located approximately 1 km offshore from the site (Figure 1A) to avoid modelling inaccuracies associated with very shallow water at low tides. The model generates wave statistics at the study site before, during and after the storm (Figures 3A–3C). The predicted sea states are a statistical representation of each three-hour period, and there will therefore be a significant number of larger individual waves within each period. The largest wave in each three-hour period, H_{max}, was predicted using a standard ratio of H_{max} approximately equal to $2 \times H_s$ (Holthuijsen, 2007), output from the model is shown in Figure 4. The SWAN model output was validated against three-hourly wave buoy data from Minehead (Figure 4A) and shows a close correlation with model results (Figures 3A and 3B). This validated SWAN wave model output is the best available wave data that were possible to collect within the scope of this project. This resolution of data enables us to examine boulder movements we measured within the wave conditions near the site during the storm. It thus assumes that wave conditions are broadly similar for our entire site and boulder sample.

Boulder population dynamics

Past observations have demonstrated that boulder populations along this coast can be highly dynamic over short periods (< one week), and that, over time, shore platforms can erode (Naylor and Stephenson, 2010), boulders are quarried (Naylor *et al.*, 2012) and rock breakdown occurs (Stephenson and Naylor, 2011). Repeat photographs from the study area illustrate the effects of this storm event on boulder dynamics most notably in boulder traps and in the boulder beach at the cliff-platform junction (Figures 2, 4).

Boulder selection and monitoring

The clasts reported here form part of a longer-term study. The boulders discussed here were quarried from the intertidal shore platform between 12 November 2007 and 11 March 2008 and were all initially of fine-medium boulder (0.25–1.0 m *b*-axis) size (Blair and McPherson, 1999). As boulder size is strongly affected by bedding properties (Stephenson and Naylor, 2011), we restricted our sample to boulders from two broadly similar beds (L19 and L24) to maintain homogeneity. On the first day of monitoring under pre-storm conditions (9 March 2008) 48 clasts were relocated: 46 were medium-fine boulders and two

A *9 March 2008*

B *12 March 2008*
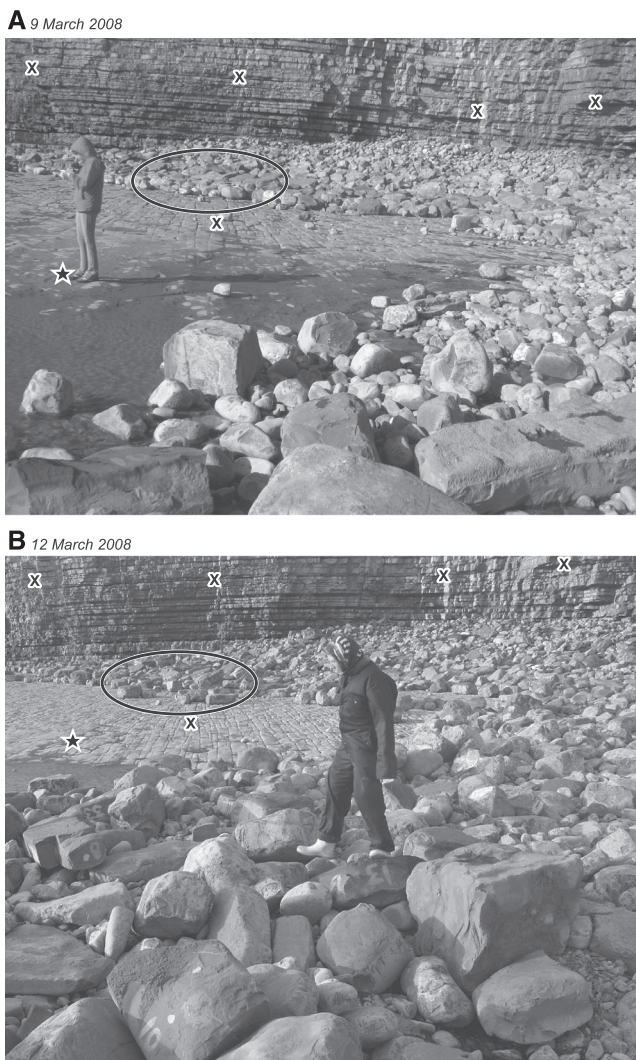
Figure 2. Paired photographs showing pre-storm (9 March) and waning storm (12 March) morphological changes in the boulder trap and boulder beach where the asterisks, oval circle and the black and white crosses serve as reference points between the two photographs. The photographs were taken using different cameras, which caused subtle differences in position.

Table I. Description of the main morphogenic zones present on the shore platform studied.

Morphogenic zone	Position on shore	Zone characteristics	Figure	Selected relevant references
Boulder trap	Across the intertidal zone apart from the cliff-platform junction	Accumulations of boulders where discontinuities such as large joints, faults or platform layer edges provide a break of slope such at boulders accumulate. This creates a stepped surface on shore platforms where boulders get trapped at the boundary between two steps. Accumulations can also form where erosion has created gaps within a platform bed. These accumulations are typically thin (< 0.75 m thick), where vertical packing is no more than three boulders thick. They range in length and width (e.g. ~5–20 m in length) depending on local geomorphological control.	2, 3 and 6	Peréz-Alberti and Trenhaile, 2015; Cruslock *et al.*, 2010
Boulder beach	At the cliff-platform junction	Beach deposit of coarse material including boulders and cobble-sized clasts, at the cliff-platform junction where beach depth is typically between 3 and 6 m. Under non-storm conditions these beaches display a cliff-top fining trend analogous to landward fining of unconstrained boulder beaches.	2 and 3	Nott, 2011. Paris *et al.*, 2011
Shore platform	Extending from low water to the cliff base.	Contiguous areas of shore platform bed layers ranging from 10^1 to 10^2 m width alongshore and up to 300 m crossshore. These surfaces typically have <25 cm difference between microtopographical high and low points and thus have a fairly smooth 'macro-roughness'. The degree of roughness varies as a function of weathering. These features typically have no or very few (< 10 boulders) resting on them apart from where boulder beaches overly the platform bed at the cliff-platform junction.		Trenhaile, 1972; Naylor *et al.*, 2012

were coarse cobbles which were parts of fine boulders that had broken between field visits (hereafter called boulders). The severity of the storm reduced the duration of the low tide sampling window to a maximum of six hours and limited the range of field measurement techniques (e.g. it was too windy for drones). During this short sampling window each day, boulders had to be relocated within a 0.1 km² study area and all daily observations, photographs and measurements taken. As such, the initial sample size was limited to the clasts found under pre-storm conditions ($n = 48$) as well those that were quarried from monitored bed layers (L19 and L24) during the storm ($n = 3$).

Daily, non-autonomous field measurements are the highest possible resolution of data that can be collected to measure boulder transport morphodynamics in the intertidal zone, as real-time 'smart pebbles' are still being developed (Maniatis *et al.*, 2013). This is because other technologies are not suitable for the harsh environmental conditions in coastal settings, including alternate wetting and drying. For examples, drifters which are used in rivers cannot be readily attached to rocks (Stockdale *et al.*, 2008) and given the mobile, saltating nature of the boulders they would be unlikely to withstand hostile rock coast conditions. Motion sensors (McNamara and Borden, 2004) can log the frequency and timing of movement over short periods of time (i.e. up to 1.5 hours of data) but not the distance and direction travelled. Other electronic tagging systems such as RFID (radio-frequency identification) and marine paint are passive (Allan *et al.*, 2006; Curtiss *et al.*, 2009) and as such daily measurement of boulder positions can only be obtained through repeat field surveying. Therefore, daily at low tide in daylight is the highest temporal resolution of boulder dynamics currently obtainable. Boulders were marked and numbered with marine paint to aid relocation. Marine

paint was used in preference to RFID tagging for two reasons. First, the large daily survey area (0.1 km²) would have been impossible to search and position with differential global positioning system (DGPS) within six hours, even with multiple RFID units operating. Second and perhaps more critically, these boulders were platform-derived and we did not want to increase the risk of wave quarrying by drilling into platform edges to deploy RFID tags. Additionally, past field observations demonstrate that boulders are often broken into smaller fragments between monitoring visits. Marine paint markings greatly improve identification of these fragments compared to RFID, which would only tag the fragment the tag was set into and may get damaged through shock during clast breakdown.

Daily position and movement patterns of boulders were recorded during daytime low tide on 9–13 March 2008 using photographs and a DGPS (10 mm *x*, *y*, *z* accuracy). This included recording the orientation of each boulder (top, bottom or side), any evidence of percussion marks or damage between days and re-measurement of boulder size where they were quarried or broken down. For days where wind conditions restricted DGPS use, boulder coordinates were obtained retrospectively using photographs to aid re-positioning. Weather conditions permitted DGPS measurements on the 11 and 13 March; DGPS data for 9, 10 and 12 March were collected post-storm, using photographs to aid re-positioning. The morphological characteristics of the platforms meant that the accuracy of re-positioned boulders was typically 0.25 m and up to 2 m in the boulder traps. This is still far better data resolution than a hand-held GPS (e.g. 3.5 m). Data were plotted in ARCGIS using python scripts to calculate direction travelled. A trigonometry-based visual basic tool was created to calculate distance travelled relative to *a*-axis of grain size and root mean
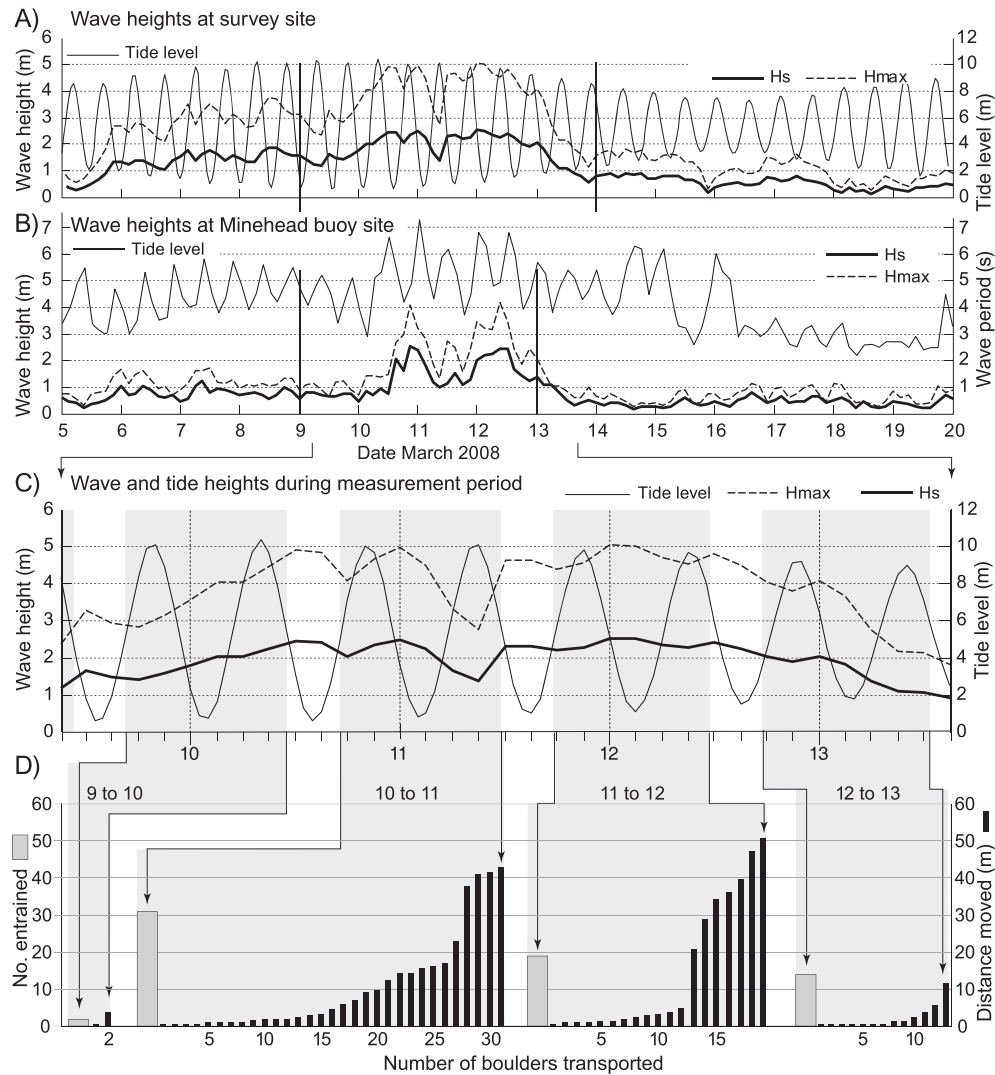
Figure 3. Wave outputs from a SWAN wave model for 16 days depicting patterns pre-storm, during and post-storm near the study site, where: (A) modelled wave data, (B) three-hourly recorded H_s and H_{max} data from the calibration site at Minehead, (C) detailed day during the five-day storm (grey = time between surveys; white = survey period) and (D) depicts daily patterns of clast entrainment (number entrained) and distance travelled by individual boulders.

squared (RMS) measurement error. RMS was calculated as the combined GPS, rover pole positioning and re-measurement (for 9, 10 and 12 March only) error. To account for the RMS error associated with each measurement type, trigonometry was then used to calculate the longest and shortest possible paths that the boulder could have travelled between two or more time intervals. This method is similar to the certainty circles used by Google Maps when assigning confidence to your location (Lutz, 2011). Paths were generated for overall net transport distance (i.e. start and end of the storm) and daily point to point (excluding position errors) measurements, where the shortest and longest routes possible to connect to/through each of the 'certainty circles' were calculated. These error path calculations allowed us to place error bars around the transport distance measured which is not typically done for coarse sediment transport measurements in any geomorphic setting. This method allows users to combine data collected using variable accuracy (e.g. drone, GPS, DGPS, photographic reconstruction and re-positioning, safety issues requiring an estimated position) and account for this as part of time series analyses of sediment transport. In coarse beach and boulder studies, differentiating between entrainment and transport is often unclear. Here, a boulder was classified as transported (i.e. entrained and transported) if the distance moved, plus the combined RMS error was greater than half the *a*-axis length of each individual clast. This conservative measure of transport

was used because the dynamic nature of clast dynamics (i.e. flipping over between surveys) and the size of the clasts (too heavy to lift) meant it was impossible to re-survey the same position on each boulder during repeat monitoring.

Factors controlling boulder entrainment

Existing theories, laboratory experiments, numerical equations and environmental reconstruction field data suggest that clast size and shape, transport mode, pre-transport setting and slope are important factors controlling boulder entrainment and transport (Nott, 2003; Imamura *et al.*, 2008; Goto *et al.*, 2011; Nandasena *et al.*, 2011). To verify this, we collected daily data for all of these clast parameters, apart from slope and pre-transport setting. Platform slope was consistent across the study area and daily low tide data were not of sufficient resolution to quantify pre-transport setting. We analysed the remaining clast properties using conventional metrics: boulder weight (metric tonnes) for size; clast dimensions (*a*, *b* and *c* axes) and Zingg for shape (after Stephenson and Naylor, 2011); boulder orientation (i.e. whether a boulder was on its top, bottom or side) and repeat photographs for transport mode. Nandasena *et al.* (2013) also suggest that topography is an important parameter for forward modelling studies predicting boulder entrainment whilst Weiss

9 – 11 March 2008   11 – 12 March 2008
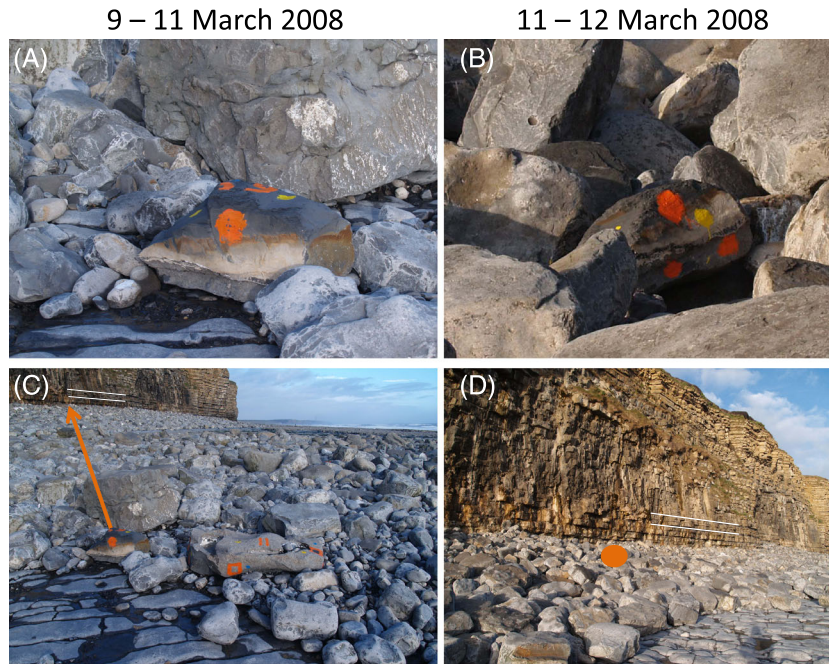
Figure 4. (A)–(D) Photographs comparing boulder trap and boulder beach morphological changes between 10 and 11 March 2008 where the white lines in (C) and (D) identify the same bed layer in the cliff showing the change in beach height and beach clast sorting between the two days; (A) and (B) also illustrate the change in position of boulder 6 and the lack of obvious damage and percussion marks, providing visual evidence that boulder 6 was carried in suspension and individual clast position.

and Diplas (2015) suggest that roughness is a critical factor influencing dislodgement of boulders during storms.

We added an additional parameter – geomorphological control which are the geomorphological controls on pre-transport, transport and depositional setting of entrained clasts. We feel this differs slightly from the term 'geomorphological setting' as geomorphological control refers to how variations in geomorphological settings across space and/or through time control other geomorphic processes (such as boulder entrainment) operating on a geomorphic template. As it was not possible to deploy a terrestrial laser scanner under these storm conditions, observations of the effects of roughness and topography on boulder dislodgement, entrainment and transport are made here. To do this we classified different morphological zones on the shore platform (Figures 1C and 2) and evaluated the effects of these different geomorphological settings on entrainment and transport. This differs from pre-transport setting of Nott (2003), which is concerned with the geological (e.g. joint-bounded) and/or hydrodynamic position of a clast prior to entrainment. It also allowed us to examine the control 'microtopographical effects' and 'macro-roughness' have on boulder transport, a parameter that is often disregarded in inverse (i.e. reconstruction of past event) models (Nandasena *et al.*, 2011; Nandasena *et al.*, 2013). Recently, Weiss and Diplas (2015) demonstrates that both bed roughness and slope angle are critically important parameters influencing the likelihood of entrainment (which they call dislodgement) by storm and tsunami waves. They argue that 'careful field observations' are required to help parameterize roughness, which they argue is 'inherently difficult to determine' (Weiss and Diplas, 2015, p. 897). Here, we demonstrate that geomorphological setting is a key determinant of these parameters.

We recorded geomorphological control on boulders daily, classifying boulder position by morphogenic zone. The relative transport distances and rates expected for each morphogenic zone (Table I) were hypothesized, as follows:

1. Shore platforms with very few loose boulders strewn on them, suggesting that boulder transport across these relatively smooth (low roughness) surfaces would be relatively rapid where the distance transported would be affected by geomorphic control in the direction of travel.

2. Boulder traps are accumulations of cobble-boulder sized clasts (moderate to high roughness properties) that are trapped along fault lines or morphological features such as shore platform layer edges which are higher than the platform layer they are resting on (see Figures 1C and 1D). We expect boulders here to have long residency times (i.e. > one year) and the shortest transport distances, especially in larger traps.

3. Boulder beaches at the cliff-platform junction. These have a high slope angle (~30°) and we have observed boulder transport over long distances over relatively short-time periods (e.g. 200 m in less than three months). We would expect transport distances here to be greatest due to fewer geomorphological controls (although where present, cliff falls may impede the rate and distance transported).

Results

Wave modelling

SWAN model outputs show that waves reached a maximum height of 5 m at the model output site 1 km offshore during the most intense part of the storm between 10 and 12 March 2008 (Figures 1A, 3A and 3C); these data were closely correlated with wave statistics from the nearest buoy (Figure 3B). The data are also comparable to modelled predictions of storm surge heights for 10 March 2008 made for the inner Bristol Channel less than 10 km upstream of the study site (Lewis *et al.*, 2011). The maximum H_s predicted was 5.05 m, and T_z up to 5.9 seconds. The data can be grouped into three storm phases: (1) building storm with H_{max} 3.5 m (9 March); (2) intense storm with H_{max} 5 m (10–12 March); (3) waning storm with H_{max} 4 m (13 March) (Figure 3C). The wave direction throughout the storm was predominantly westerly (240°–290°); suggesting a west to east boulder transport direction.

The intensity of these waves was compared to the recent extreme storms of 2013 to 2014. During this storm, the highest wave height recorded at the closest buoy (Minehead, (5.96 m H_{max}) was nearly 2 m higher than the largest wave (4.06 m on 9 February 2014) during the recent exceptionally stormy winter of 2013 to 2014 [Met Office, 2014; Channel Coast Observatory, 2015, respectively]. It is also over 1 m higher than the next highest wave recorded during the 2007–2008 winter at Minehead (Channel Coast Observatory, 2015). Between November 2007 and March 2008, there were 23 individual waves with H_{max} values greater than 4 m and 69 waves with a H_{max} greater than 3.5 m, which is 1 m above the storm threshold for this area. Forty-eight percent of waves greater than 4 m and 41% of waves greater than 3.5 m occurred between 10 and 12 March 2008, showing the intensity and high magnitude of this storm event within a particularly stormy winter (cf. Turton and Fenna, 2008).

Boulder dynamics

Repeat photographic analysis of pre-storm, during and post-storm data was used to demonstrate how the storm influenced boulder dynamics in key morphodynamic zones. Figures 2A and 2B and Figures 4A–4D clearly illustrate that the shape and composition of boulder traps and boulder beaches were radically altered during the storm. For example, the boulder trap in front of the person in Figure 2A shows changes in boulder orientation and in the number of clasts in the trap between pre-storm conditions (9 March) and waning storm conditions (12 March). Similarly, the oval circles in Figure 2 and comparative lines in Figures 4C and 4D show changes in the composition of the boulder beach between the two dates. The composition of the boulder beach during the waning storm is more mixed, with larger, imbricated boulders located towards the top of the beach compared to a more stratified beach with larger amount of fine boulders at the beach apex under pre-storm conditions (Figures 2, 3). The beach height was also notably lower after the most intense day of the storm (Figure 4). This provides strong evidence of storm-based reworking of boulder beaches and boulder traps during storm events. It is within the context of this highly dynamic setting that our individually tagged boulders were monitored to provide quantitative evidence of boulder entrainment, transport and breakdown during the storm.

Individual boulder entrainment and transport patterns varied considerably during the storm where different boulders were often recorded on individual days. Table II summarizes the boulder characteristics across all days, as well as immediately pre- and post-storm. Five boulders were also produced during the storm, three from quarrying of the intertidal shore platform and two arising from one boulder that broke into three pieces between 10 and 11 March. This increased the total sample size at the end of the storm to 53 (Table II).

Responsiveness of boulders to wave climate variations during the storm

The data strongly suggests that there are strong interactions between wave properties and boulder dynamics including entrainment, transport, quarrying and breakdown. Of the 48 boulders monitored from the start of the storm, all but three were entrained and transported at some point during the storm (= 94% entrained). This suggests there is a strong positive correlation between storm wave characteristics and boulder dynamics. When daily entrainment patterns (Figure 3D) are compared with wave statistics (Figure 3C), it is evident that entrainment frequency is closely aligned to wave parameters. Entrainment was minimal (6%) while the storm was building (9–10 March), peaked on the two intense days of the storm (10–12 March), and then declined on the 12–13 March (Table II, Figures 3C and 3D). Transport dynamics mirrored entrainment patterns – more boulders were transported over a greater distance on the most intense days of the storm (Figures 3C and 3D). Critically, all boulders that were entrained were also transported. Using our criteria, transport equals a minimum of half the axis dimension of the boulder ± RMS measurement error. All quarrying and rock breakdown also occurred during the two most intense days of the storm – showing that higher wave energies were required to dislodge, entrain and transport intact rocks [that were joint-bounded on two or three sides, see Naylor et al. (2012) for photographic evidence] and cause rock breakdown where one boulder broke into three pieces. During the two most intense days, there is a clear step change in transport distance, above and below 20 m (Figure 3D). In subsequent sections, we attempt to elucidate which parameters might be controlling the clustering of boulder transport into two distinct groups. It is also noteworthy that the three boulders that were not entrained were firmly wedged within small boulder traps for which entrainment would have required very high, prolonged lift forces (Weiss and Diplas, 2015).

Table II. Summary of boulder entrainment and transport characteristics for pre-storm, during and post-storm conditions.

Storm condition	Monitoring date	Sample size (n)[a]	Number of clasts						Percentage recovered (%)
			Relocated	Not moved	Entrained	Transported	Quarried	Broken	
Data derived from comparing between two dates[b]									
Before	9 March	48	39	3[c]	n/a	n/a	n/a	n/a	n/a
Intense	10 March	48	35	33	2	2	0	0	6
Intense	11 March	51	37	6	31	31	1	1[d]	84
Intense	12 March	53	34	15	19	19	2	0	56
After	13 March	53	34	21	13	13	0	0	38
Data derived from comparing the first and last monitoring day									
Before and after	9, 13 March	48	39	3	36	36	0	1	81

[a]Maximum possible number of boulders in our re-survey population that could be found.
[b]Dates compared are the row above and the row the data is entered in.
[c]Not moved during the entire storm rather than between two days;
[d]One boulder was broken into three pieces.
Note: n/a, not available.

Net transport distance

Thirty-nine boulders were found on the first and last day of monitoring, immediately before and after the storm (Table II). We calculated the distance moved between the first and last day of monitoring which we term the net transport distance (NTD). As not all of these boulders were found each day during the storm, it was not possible to calculate the actual distance transported (i.e. sum of the distance transported per day). The NTD of these boulders is discussed further. Statistical analysis of the relationship between NTD and boulder size (weight, metric tonnes) determined that there is no relationship between boulder size and NTD (Spearman's Rank significance =0.887; $n = 39$). Figure 5A illustrates considerable variability and little evidence for a relationship between boulder weight, size and distance transported during the storm, although there appears to be a maximum weight threshold that limits entrainment and boulder transport. The maximum weight threshold for entrainment varies considerably between morphogenic zone (Tables I, III). These results have few data points of clasts near the maximum entrainment threshold for each morphogenic zone. Nonetheless, the data suggest there is a relationship between morphogenic zone and transport distance and rate that warrants further research. Below the maximum entrainment and transport threshold, the NTD data appears to have two distinct clusters between 0 and 17 m and 35–45 m. Our data does not demonstrate the strong fining trend of weight versus distance demonstrated by Goto *et al.* (2011), suggesting that boulder size is not responsible for the step-change in daily transport observed in Figure 3D during an intense extratropical storm. One pair of boulders was found daily (2.1 and 2.2), allowing a comparison between gross daily transport and NTD to be made. Boulder 2.2 is a smaller coarse cobble sized clast that originally was part of now much larger boulder 2.1, yet it moved a much shorter distance than boulder 2.1 which was clearly dragged landward via swash before
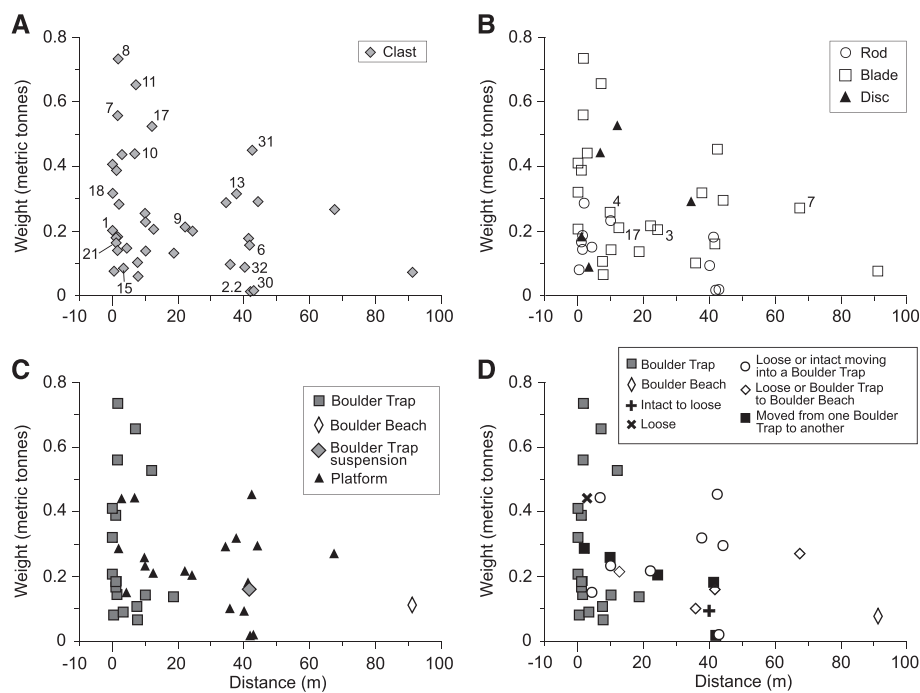
Figure 5. (A)–(D) Net transport distance ($n = 39$) between 9 and 13 March, where distance was plotted against size (= weight, metric tonnes) and grouped as follows: 4 A size; 4B by shape type; 4C dominant transport surface type and 4D pre- and post-transport geomorphological control, where selected boulders are identified by number where in panels A they are from the L24 study area and in panel in panel B from the L19 study area. See legends on individual figures for an explanation of the symbols.

Table III. Showing the relationship between maximum entrainment threshold weight, geomorphological controls on boulder transport and hypothesized transport rates and distances.

| Morphogenic zone (pre- and post-transport)	Transport surface	Hypothesized transport rate	Hypothesized transport distance	Maximum entrainment/ transport threshold (metric tonnes)	Distance transported (m ± RMS error)
Boulder trap	Boulder trap (*moved within one boulder trap*)	Slowest	Shortest	0.73	1.65 ± 0.11
Boulder trap to boulder trap	Shore platform (*moved between two boulder traps*)	Fast during movement across shore platforms	Variable, depending on distance between boulder traps	0.45	42.37 ± 0.11
Platform to boulder beach	Shore platform and boulder beach (*moved across platform onto the beach*)	Fast	Not hypothesized	0.27	67.39 ± 0.11
Boulder beach	Boulder beach (*moved along the beach*)	Fastest	Greatest	0.07	91.12 ± 0.61

being shifted alongshore via backwash (Figure 6). These results show that gross transport distance was 38% greater for the larger of the two clasts. The results suggest that boulder shape and size do not control boulder entrainment and transport distance.

Transport mode

Daily observations were of high-enough resolution to identify some modes of boulder transport [i.e. rolling after Nandasena *et al.* (2013) and suspension after Hansom *et al.* (2008) for individual boulders. Some terminology differs between authors where Nandasena *et al.* (2013) refer to an orientation changed by 180° over the long axis as rolling whereas Imamura *et al.* (2008 refer to this as flipping). For consistency, we have used the term roll. In many cases daily observations were not frequent enough to confirm that a boulder definitely slid or rolled, or that it moved by multiple modes, as the observational evidence could not be attributed solely to a particular mode. For some boulders a clear mode of transport was evident. For example, boulders 7, 8, 11 and 17 rolled between 10 and 11 March 2008 (Figures 5C, 7A, 7B and 8A–8E). These boulders were blade or disc shaped (i.e. platy) and ranged in weight from 0.44 to 0.73 tons. They provide field verification of laboratory experiments suggesting that platy boulders roll (Imamura *et al.*, 2008). They also suggest that the rolling equations of Nandasena *et al.* (2011, 2013) are reliable estimations as our maximum possible modelled wave height (5.05 m) was 1 m greater than the threshold calculated using their equations for these boulders.

L24 boulder 6 (0.16 tons, Figures 4, 7A and 8B) was most likely carried in suspension (above the boulder trap, Figures 4, 8B) as a visual analysis of the boulder found there was no notable erosion and other boulders (of similar shape and size) that were also positioned on the edge of the boulder trap were entrained and deposited within it on the same day (e.g. L24 boulder 3, 0.13 tons). This provides field verification of suspended boulder transport observed in wave tanks (Hansom *et al.*, 2008). It also allows us to evaluate the saltation entrainment equation of Nandasena *et al.* (2011, 2013), which is the closest parameter they model to suspension. A comparison of the maximum modelled wave height predicted during the storm (5.05 m) to Nandasena *et al.*'s (2013) saltation equation calculation for boulder 6 (6.43 m) shows that the Nandasena equations overpredicted the wave energy required to move this boulder by saltation by at least 20%.
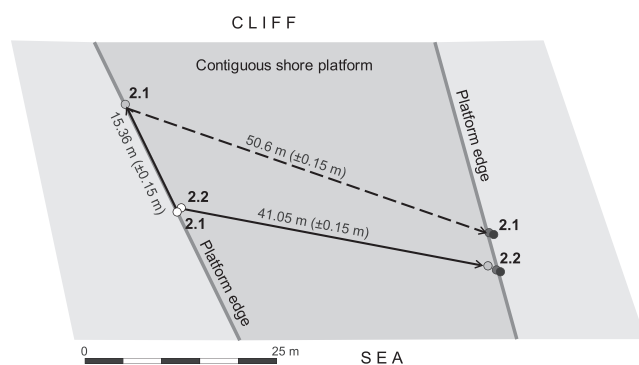
Figure 6. Depicts different daily transport distances and pathways between two boulders (2.1 and 2.2) which started (white dots) and ended (black dots) the storm in very similar places, but moved differently during the storm (i.e. grey shaded dots and dashed line), demonstrating the variability in swash and transport dynamics and the differences between gross and net transport distance.

Platform erosion and rock breakdown

Daily data was of sufficient resolution to measure shore platform erosion and rock breakdown. Three fine-medium boulders were eroded from the shore platform between 10 and 11 March ($n = 1$, number 31 in Figure 7A) and 11 and 12 March ($n = 2$, numbers 32 and 33 in Figure 7B). These boulders were quarried, entrained, lifted ~0.4 m onto a shore platform and transported 15.9 m, 39.3 m and 34.3 m, respectively, in less than 24 hours between daily visits (Figures 7A and 7B). Although this might appear to be a small number of detached boulders given the intensity of the storm, all of the boulders discussed in this paper were detached from these platform layers over the 2007–2008 winter. As such, it is possible that antecedent erosion of 'at risk' platform edges limited the quarrying that occurred during this storm (Backstrom *et al.*, 2016). In less than 24 hours between 10 and 11 March one fine boulder (0.23 tons, 0.4 m *b*-axis) was lifted from a boulder trap, moved across the shore platform, broken into three pieces and deposited in a boulder trap 9.7–14.2 m to the east. Whilst these data provide direct evidence of flipping, suspension, quarrying and breakdown; the mode data are not able to explain the observed thresholds in boulder movement during the most intense days of the storm (Figure 4D).

Geomorphological Control on Boulder Dynamics

The lack of a clear trend between size, shape, mode and transport distance leads us to ask: What else might be controlling boulder transport dynamics? It has been suggested that local morphological variations (e.g. surface irregularities, bed roughness, macro-roughness or microtopography) influence entrainment and transport distance during storms and tsunamis (Noormets *et al.*, 2004; Hansom *et al.*, 2008; Imamura *et al.*, 2008; Nandasena *et al.*, 2013; Terry *et al.*, 2013; Weiss and Diplas, 2015). The scale of these roughness parameters is typically weakly described by the authors, although Nandasena *et al.* (2013) use a Manning's formula of 0.025 and suggest that macro-roughness may have obstructed boulder movement. There is no conclusive field data demonstrating the effects of bed roughness on boulder entrainment and transport. Using daily field data, we assessed the effects of geomorphological control in two ways: (1) the dominant surface type across which boulder transport occurred and (2) the pre- and post-transport morphogenic zones. Here, the roughness varies from 10^1 to 10^2 cm between the different morphological zones boulders moved across (Table I).

When total transport distance data are disaggregated by dominant transport surface (Figure 5B) two parts of the dataset (below the maximum size threshold) become clearer. First, boulders that stayed within one boulder trap moved the least distance; this explains much of the first cluster of data between 0 and 17 m on Figure 3D. Second, the boulder that moved entirely within the boulder beach moved furthest [91.1 ± 0.6 m (0.4 m *b*-axis, 0.07 tons, fine-boulder, Figure 5C)]. The pattern within the shore platform morphogenic zone appears less conclusive (Figure 4B) as some boulders moved very little and others moved some distance. To unravel this complex behaviour, the data were grouped into pre- and post-transport morphogenic zones (Figure 5C). There were five types of pre- and post-transport settings with a shore platform as the dominant transport surface. These were: (a) to a boulder trap ($n = 10$); (b) between two boulder traps ($n = 5$); (c) to a boulder beach ($n = 3$); (d) remained loose on the platform ($n = 1$,
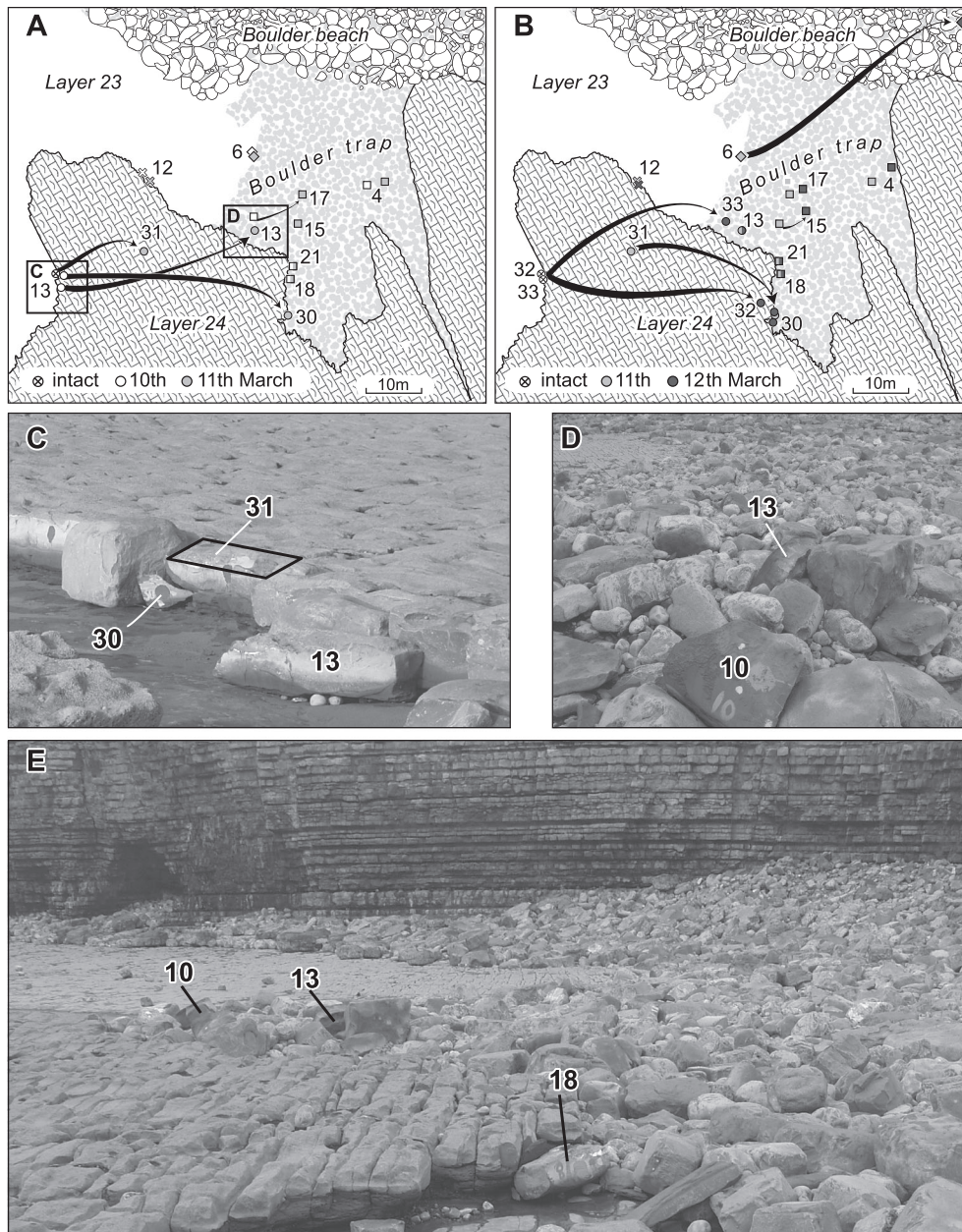
Figure 7. (A)–(E) Depicts movement patterns of selected boulders during the most intense periods of the storm.

B12, Figures 7A and 7B, which was sheltered from dominant waves); (e) from intact to loose on the platform (*n* = 1). Of these, types (a) and (b) are most common and discussed further.

Analysis of the boulders (*n* = 10) that moved to a boulder trap is insightful (Figure 5D). Half of the rocks moved less than 20 m and the remainder formed part of the second cluster of boulders that were transported between 35 and 45 m on the most intense days of the storm (Figure 3C). The reason for these two clusters is the difference in the spacing of boulder traps for each cluster of boulders; boulders 13, 30–33 in Figures 7A–7E illustrate the second cluster well. The spacing of different morphogenic zones also explains the dispersion of data for boulders that moved between two boulder traps and the step change in boulder transport observed in Figure 3D.

Comparisons of pairs of boulders between daily site visits provide observational evidence of the critical role geomorphological control plays in boulder dynamics. In the absence of real-time instrumentation of platform wave dynamics (which were not possible to deploy during the storm) and individual boulders (emerging technologies such as smart pebble sensors are still not yet available for this application, e.g. Maniatis

et al., 2013), this was the highest temporal resolution and level of quantification that was possible to collect. Ten pairs of boulders that had near identical weights but different pre-transport geomorphological settings illustrate geomorphological control (Table IV). A few key pairs are discussed in detail here.

The effect of pre-transport geomorphic setting and transport surface morphology on boulder transport distance is apparent when boulders of similar weight but different pre-transport geomorphic settings are compared. Three examples are used to illustrate this point, using Figure 5B for weight and Figures 7B–7E for pre-transport setting. One pair of blade-shaped boulders of identical size (0.32 tons) and shape but different pre-transport geomorphic settings shows that pre-transport setting, transport surface morphology and post-transport geomorphic setting exerts a strong control on both daily movements and the NTD over the entire storm. Boulder 13 was initially loose on L23 platform and was entrained, lifted onto the next bedding layer (L24, ~0.4 m elevation change, Figures 1C, 1D and 7A) and transported 37.7 ± 0.11 m on 10–11 March whereas boulder 18 was wedged in a boulder trap and did not move during the storm (Figures 7C, 8A and 8B). Thus boulder 13 had more
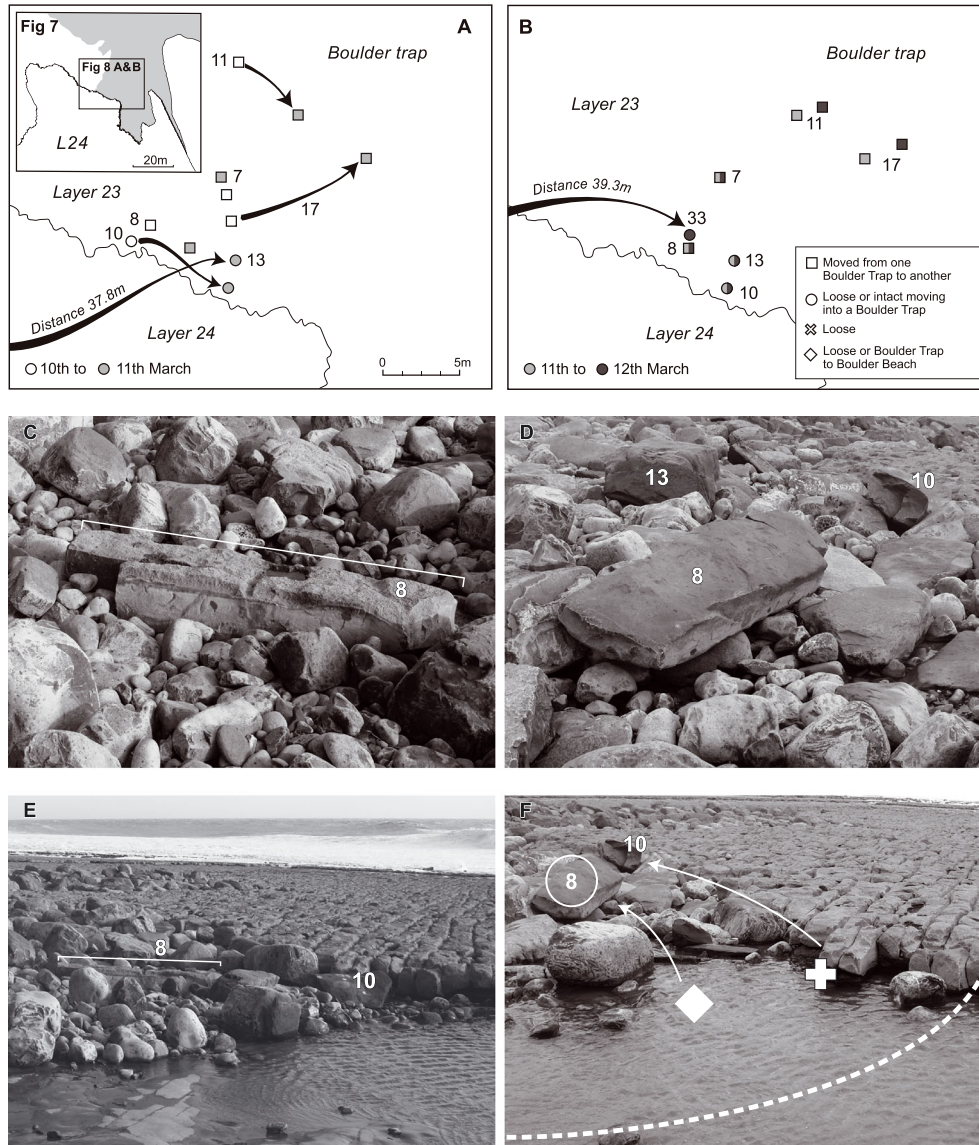
Figure 8. Maps showing boulder movement during the storm where: (A) shows boulders that flipped (squares, weighing between 0.52 and 0.73 tons) between 10 and 11 March, boulder 10 (0.44 tons) which slid and boulder 13 (0.32 tons, multiple possible transport modes); (B) differential movement trends mapped between 11 and 12 March; (C) shows boulder 8 (0.73 tons) on 10 March; (D) the same rock on 11 March, demonstrating that it flipped; (E) shows where boulder 8 moved from (white diamond, which was loose on the platform, near the western edge of the boulder trap = dashed black line) and to (white circle) in <24 hours. The dashed line also illustrates how much the entire boulder trap edge shifted in <24 hours.

suitable pre-transport and transport surface morphologies which allowed this boulder to move 37 times further than boulder 18 which was geomorphologically constrained (Figure 7E). Boulders 10 and 31 further illustrate these effects. They are nearly the same weight (0.44 and 0.45 tons, respectively), yet the distances transported between 10 and 11 March (6.74 ± 0.06 and 15.9 ± 0.1 m, respectively) and between the start and end of the storm (Figure 7B), were very different (Figures 8B–8E). Boulder 10 was loose on the western edge of the boulder trap on 10 March and slid into the boulder trap on 11 March whereas boulder 31 was intact on 10 March, was quarried from a joint-bounded setting, lifted onto L24 and transported 15.9 m over the same time period. This shows that the geographic proximity of boulder 10 to the boulder trap (Figures 8D and 8E) restricted the distance travelled. It also shows that the total distance travelled by boulder 13 was constrained by the boulder trap as similar wave dynamics on the second intense day of the storm were not sufficient to entrain this boulder (Figure 8B), providing strong evidence of geomorphological control. Meanwhile, boulder 12 of similar weight to both boulders 10 and 31 (0.44 tons, Figures 7B, 8B, and 8C) was loose on the platform but only

moved a limited distance during the five-day survey period (2.81 ± 0.1 m). This is most likely due to its pre-transport position, being adjacent to the edge of L24 and thus in relative shelter from the incoming waves (as well as L24 restricting movement during backwash). For boulder 31, although more force would have been required to detach, entrain and lift the clast onto L24 as well as transport it, it moved over two times further than boulder 10 between 10 and 11 March (Figure 8B) and again between 11 and 12 March (Figure 8C) until it was deposited into the boulder trap. In total, boulder 31 moved 42.4 m, over six times further than boulder 10. This shows that platform morphology in the direction of travel exerts a strong control on the distance transported where the presence of a boulder trap restricts total transport distance more than shape and size. Boulders 6 and 21 show that pre-transport geomorphic setting has a strong control over entrainment. These boulders are of equal weight (0.16 tons), where boulder 6 was loose on the western edge of a boulder trap and boulder 21 was situated in a narrow section of the same boulder trap on 10 March 2008 (Figure 8B). Both rocks moved a small amount between the 10 and 11 March 2008 (boulder 6 = 1.21 ± 0.6 m and boulder 21 = 0.5 ± 0.1 m,

Table IV. Summary data comparing pairs of similarly sized and shaped boulders with different net transport distances.

Pair	Boulder number	Shape class	Weight (t)	Pre-transport setting	Transport surface	Post-transport setting	NTD (m)	Difference[a]	Figure	Interpretation (dates in brackets)
1	6	Blade	0.16	BT edge	BT	BB	41.6	39× greater	4 A–4B, 5 A–5E	Discussed in text earlier.
	21	Rod	0.16	BT	BT	BT	1.1			
2	10	Disc	0.44	P	P, BT	BT	6.8	6.3× greater	4 A–4B, 5 A–5E	Discussed in text earlier.
	31	Blade	0.45	I	P	P, BT	42.4			
3	13	Blade	0.32	P	P	BT	37.7	38× greater	4 A–4B, 5 A–5E, 6D	Discussed in text earlier.
	18	Blade	0.32	BT	BT	BT	0.0			
4	32	Disc	0.09	I	P	P	40	12× greater	4 A and 5 A	B32 was an intact, joint-bounded boulder (9–11). It detached (11–12) and was repeatedly entrained finishing the storm <3m from a BT. B15 moved 12× less as it was confined to a large BT.
	15	Rod	0.09	BT	BT	BT	3.3			
5	7	Blade	0.52	BT edge	BT	BT	1.6	7.7× greater	4 A and 6 A–6B	Differential boulder movement within a BT where B17 moved 7.7× further and was loosely packed on the edge of the BT whereas B7 was within it.
	17	Disc	0.56	BT	BT	BT	12			
6	8	Blade	0.73	BT	BT	BT	7.0	4.3× greater	4 A, 6 A–6E	Both rocks moved very little within a BT, but B8 moved 4.3× further despite being heavier.
	11	Blade	0.65	BT	BT	BT	1.7			
7	2.2	Rod	0.014	BT	Platform	BT	41.9	0× greater	4 A and 5 A–5C	This pair moved between two BTs with similar spacing between them, yielding similar net transport distances.
	30	Rod	0.016	Loose	Platform	BT	42.9			
8	1	Rod	0.20	BT	BT	BT	0	22× greater	4 A	B1 was wedged within a small BT whereas B9 was on the western (wave front) edge of a large BT that was loosely packed, enabling greater transport.
	9	Rod	0.21	BT	BT	BT	22.0			
9[b]	3	Blade	0.20	BT	P	BB	24.2	2× greater	4B	B17 moved between two BTs; this constrained transport compared with B3, which started in a BT and moved into the BB.
	17	Blade	0.21	BT	P	BT	12.4			
10[b]	4	Blade	0.26	BT	P	BT	9.8	6.9× greater	4B	B7 was repeatedly transported, moving from a BT to the BB (10–11) and along the BB thereafter. B4 moved between two BTs.
	7	Bblade	0.27	BT	P	BB	67.4			

Note: BT, boulder trap; BB, boulder beach; I, intact; P, platform.
[a]The × times greater is the ratio between the distance transported between each pair.
[b]Derived from L19.

Figure 7B). However, between the 11 and 12 March, boulder 6 was moved from the western edge of the boulder trap (Figure 7B), transported 46.8 ± 0.1 m in suspension and deposited in the boulder beach at the cliff-platform junction whereas boulder 21 did not move (Figure 7C).

These data support our hypotheses as boulder residency times are greatest and transport is slowest in boulder traps, whereas boulder beaches are zones of fairly rapid cross and longshore transport. Shore platforms are zones of fairly rapid longshore transport resulting in limited scope for deposition ($n = 2$ at the end of monitoring), where NTD is limited by the spacing of boulder traps. These comparisons also show that boulder entrainment and NTD is often limited by the presence of boulder traps, showing that bed roughness can limit entrainment and that post-transport geomorphological setting is a key determinant of transport distance. These comparisons also show entrainment and transport is often limited by the presence of boulder traps, providing field verification that macro bed roughness (i.e. between 10^1 and 10^2 cm) is an important control on entrainment (validating Weiss and Diplas, 2015) and demonstrating that post-transport geomorphological setting is a key determinant of total transport distance. Our results also show that position relative to the boulder trap seems to affect the amount of transport during a multi-day storm event, where loosing packed boulders on the edge exposed to incoming waves were transported further than similar sized and shaped boulders further into the boulder trap, suggesting that position and packing are further controls within trap transport dynamics. Further fieldwork is needed to quantify residence times within the boulder traps, factors controlling their formation and change (e.g. erosion of platform bed edge creating a trap) and their role in supplying clasts to the boulder beach. With sufficiently large datasets in multiple types of each morphogenic zone, it may be possible to predict movement probability and thus improve transport equations.

To quantify the localized effects of morphological zones on wave attenuation, a multiple array of pressure transducers and directional wave recorders would be required across the study site, which was beyond the scope of this study. Thus, our data allow us to show that boulder traps influence total transport distance under the same broad wave conditions that were modelled for the entire site, suggesting that the boulder trap exerts a strong role on boulder transport (and that this may also include localized attenuation of wave power).

Stormy Geomorphology – How Frequent are Storms Like This One?

Earlier we noted that the 10–12 March 2008 storm was particularly intense within one winter and compared to the recent 2013–2014 storms. The question remains as to how much of an outlier this storm event is? Using the best available local data, we have placed this storm within the instrumental record of storm surges and offshore wave characteristics. At nearby Avonmouth, 10 March 2008 was registered as the fourth largest extreme storm-tide event (8.04 m) in a 14-year record (1994–2008) (Lewis *et al.*, 2011). This surge was one of 17 recorded over a 14-year monitoring period (Lewis *et al.*, 2011) as being greater than 15% higher than the mean high water spring tide, above 7.81 m ODN which corresponds approximately to a one in one year event (Dixon and Tawn, 1997). This demonstrates that this storm surge event, although notably large, is not rare.

Inshore wave buoys in the Bristol Channel have short data-records (~10 years in duration) and the nearest offshore wave buoy to the study area is located at Turbot bank, located off the southwest tip of Wales (Figure 1). Figure 9 places the off-shore wave climate for 2008 within the longest locally available data record (66 years), using the combined Ships of Passage (position SoP) and Turbot Bank buoy (position TB) dataset for wave height (no wave direction data were recorded). These two datasets have a short period of overlap when the TB buoy replaced the SoP light vessel in the 1990s. We pooled and cleaned these data for periods where the data was of insufficient quality, spurious or unavailable (e.g. during periods of maintenance or when the buoy was blown away) and plotted to generate a time series of waves likely to do geomorphic work: mean annual H_{max} (in metres). These data were overlain with the 10-year record from the nearest in channel buoy at Minehead,
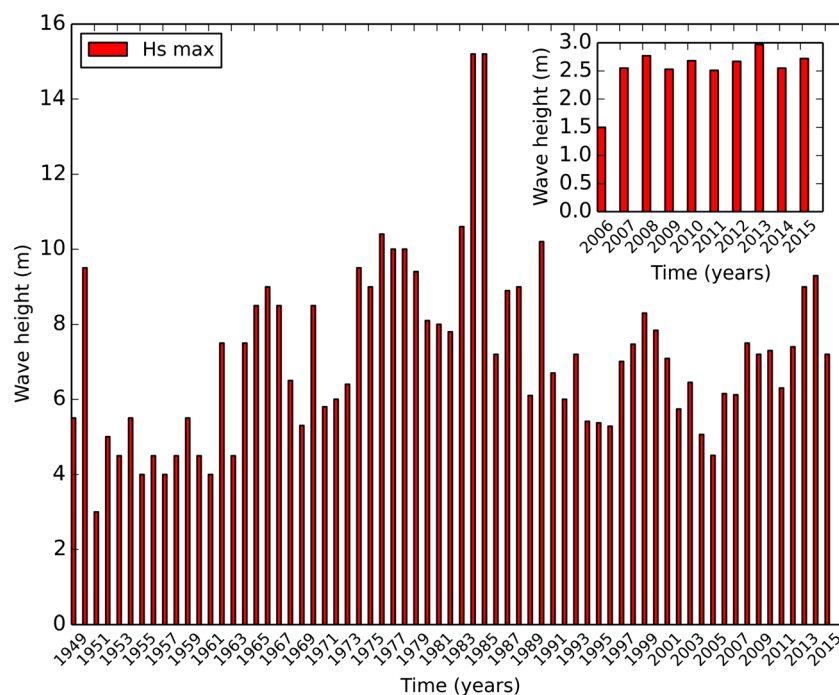
Figure 9. Time series plots of the annual H_{max} (in metres) wave height values for Turbot bank and Minehead (inset) buoys.

Table V. Calculated extreme value analysis recurrence intervals for the Turbot bank buoy.

Recurrence interval (years)	Maximum wave height (m)
1	8.77
2	9.36
5	10.13
10	10.69
20	11.25
50	11.98
100	12.52
200	13.06

which shows that two of the last 10 years had mean annual H_{max} values exceeding 2.75 m, 2008 and 2013 (Figure 9 inset).

Extreme value analyses (EVAs) are a common metric used to estimate return periods of storm events (Coles, 2001; Ortego et al., 2012). We used a Weibull analysis to calculate the maximum H_s extreme value analysis on the Turbot bank data (Table V). The calculated EVA for a one in one year event is 8.77 m, which is greater than the mean H_{max} value during 2008. This shows that the 2008 wave conditions at Turbot bank were not extreme. Why, then, did this storm cause coastal erosion and flooding from Wales to northern Spain (e.g. Cariolet et al., 2010; Feal-Pérez et al., 2014)? An unusual feature of this storm event is that the inshore waves remained large relative to the offshore conditions at Turbot bank (e.g. maximum measured waves of 7.5 m and 5.96 m on 10 March 2008 at Turbot Bank and Minehead, respectively), creating more powerful, erosive nearshore waves. This is likely related to a combination of tidal conditions, wave period and wave direction. These large nearshore waves, coupled with the intensity and persistence of large waves over the storm event described earlier, appear to be key parameters controlling geomorphic work on rock coasts. These data also illustrate the dearth of robust, long-term instrumental datasets in the inshore or nearshore environments; these are necessary to calculate recurrence intervals for storm events that cause substantive geomorphic change, and the human impacts often associated with them.

Conclusions and Future Research Needs

Several key findings and future research directions emerge from this research. Our data provide the first known data demonstrating daily entrainment and transport of shore-platform derived boulders during a storm event. These data show that intertidal boulders can be repeatedly entrained, transported and deposited during a multi-day storm event and that some boulders are broken into smaller clasts. As the boulders measured are all platform-derived, they also demonstrate that shore platforms are actively eroding and that these erosion products are actively re-worked and broken down and therefore, actively contribute to local sediment budgets.

The data also show that under high wave energy conditions for this location, all boulders that were entrained were also transported over two high tides between daily measurements. This suggests that entrainment and transport are near simultaneous. Higher-resolution monitoring once smart pebble technology is advanced sufficiently could verify this and inform modelling studies. Our field data also show that intertidal boulder transport is controlled by a suite of local geomorphological factors, in addition to wave, lift and drag forces and clast properties such as size and shape. The data illustrate that geomorphological setting – the spatial arrangement of morphogenic

zones (e.g. boulder traps) and the topographic irregularities and bed roughness this creates across a shore platform – exerts a strong control on boulder entrainment and transport distance. This parameter is not typically used when reconstructing or predicting the wave energies of tsunami and storm events, although the importance of including bed roughness and slope angle as parameters controlling entrainment has recently been argued (Weiss and Diplas, 2015). Future forward and inverse modelling studies would benefit from increasing pre-transport conditions controlling entrainment to four, by including boulders that are packed. This would be in addition to joint bounded, subaerial and submarine conditions used by Nott (2003) and Nandasena et al. (2011). These results strongly suggest that consideration of geomorphological control on boulder entrainment and transport is necessary as part of palaeo-storm and sedimentary reconstruction studies.

Our data show that daily data is not of high enough resolution to fully quantify essential parameters of boulder entrainment and transport equations; namely the wave energy causing entrainment or the range of modes during transport. Until our technological capacity improves, these data are the highest resolution obtainable. In future, once emerging smart pebble sensor technologies (Maniatis et al., 2013) are sufficiently developed, we can improve the temporal resolution of boulder data alongside detailed measurements of wave dynamics across shore platforms including differential wave transformations between morphogenic zones. These high-resolution data would allow us to link boulder entrainment and transport to specific wave conditions and to unravel whether boulders move by multiple modes and/or are transported multiple times during wave inundation. Such data are also needed to determine the localized effects of different platform morphologies and morphogenic zones on wave energy. These data would help untease just how critical geomorphological control is, and under what range of wave conditions. Detailed three-dimensional platform morphologies derived from unmanned aerial vehicles (UAVs) or terrestrial laser scanners (TLSs) would assist in interpreting and quantifying these data and inform theoretical modelling approaches.

In a changing climate, vulnerability assessments and management of rocky coasts will become more commonplace (Wong et al., 2014). Well-instrumented storm-event rock coast dynamics data combined with morphological, wave and tide factors are needed to measure rock coast erosion and to develop rock coast sediment budgets (Naylor et al., 2014) for coastal managers. Demonstration of the critical role that macro-roughness and morphogenic zones play in mediating the nature and rate of sediment transport in rock coast systems is also highly relevant for improving our ability to generate sediment budgets for rock coast systems. Further research is needed on the variability in transport between units of the same morphological zones, differential rates of movement in different zones and the rates of transfer between morphogenic zones. These measurements, along with improved measurements of shore platform and cliff erosion rates will allow us to develop rock coast sediment budgets. These data will provide important insight into the rates and volumes of material derived from rock coasts that supply coarse mixed (i.e. cobble-boulder sized clasts) beaches and barriers that protect valuable coastal assets.

References

Allan JC, Hart R, Tranquili JV. 2006. The use of Passive Integrated Transponder (PIT) tags to trace cobble transport in a mixed sand-and-gravel beach on the high-energy Oregon coast, USA. *Marine Geology* **232**: 63–86. DOI:10.1016/j.margeo.2006.07.005.

Backstrom J, Jackson D, Cooper A, Loureiro C. 2016. Contrasting geomorphological storm responses from two adjacent shorefaces. *Earth Surface Processes and Landforms.* DOI:10.1002/esp.3788.

Bidlot J-R, Holt MW. 1999. Numerical wave modelling at operational weather centres. *Coastal Engineering* **37**: 409–429. DOI:10.1016/S0378-3839(99)00036-8.

Blair TC, McPherson JG. 1999. Grain-size and textural classification of coarse sedimentary particles. *Journal of Sedimentary Research* **69**: 6–19. DOI:10.2110/jsr.69.6.

Booji N, Ris RC, Holthuijsen LH. 1999. A third-generation model for coastal regions. 1. Model description and validation. *Journal of Geophysical Research* **104**(C4): 7649–7666. DOI:10.1029/98JC02622.

Cariolet J-M, Costa S, Caspar R, Ardhuin F, Mange R, Goasguen G. 2010. Aspects météo-marins de la tempête du 10 Mars 2008 en Atlantique et en Manche. *Norois* **215**: 11–31.

Chen B, Chen Z, Stephenson WJS, Finlayson B. 2011. Morphodynamics of a boulder beach, Putuo Island, SE China coast: the role of storms and typhoon. *Marine Geology* **283**: 106–115. DOI:10.1016/j.margeo.2010.10.004.

Channel Coast Observatory. 2015. http://www.channelcoast.org/ [9 July 2015].

Coles SG. 2001. An introduction to Statistical Modelling of Extreme Values. Springer: London; 209.

Cruslock EM, Naylor LA, Foote YL, Swantesson JOH. 2010. Geomorphologic equifinality: a comparison between shore platforms in Höga Kusten and Fårö, Sweden and the Vale of Glamorgan, South Wales, UK. *Geomorphology* **114**: 78–88. DOI:10.1016/j.geomorph.2009.02.019.

Curtiss GM, Osborne PD, [a]Horner-Devine AR. 2009. Seasonal patterns of coarse sediment transport on a mixed sand and gravel beach due to vessel wakes, wind waves, and tidal currents. *Marine Geology* **259**: 73–85. DOI:10.1016/j.margeo.2008.12.009.

Dixon MJ, Tawn JA. 1997. Spatial analyses for the UK. *Proudman Oceanographic Laboratory report* **112**: 200.

Earlie CS, Young AP, Masselink G, Russell PE. 2015. Coastal cliff ground motions and response to extreme storm waves. *Geophysical Research Letters* **42**(3): 846–854. DOI:10.1002/2014GL062534.

Feal-Pérez A, Blanco-Chao R, Ferro-Vázquez C, Martínez-Cortizas A, Costa-Casais M. 2014. Late-Holocene storm imprint in a coastal sedimentary sequence (northwest Iberian coast). *Holocene* **24**(4): 477–488.

Fichaut B, Suanez S. 2011. Quarrying, transport and deposition of cliff-top storm deposits during extreme events: Banneg Island, Brittany. *Marine Geology* **283**: 36–55. DOI:10.1016/j.margeo.2010.11.003.

Foulds SA, Macklin MG. 2016. A hydrogeomorphic assessment of twenty-first century floods in the UK. *Earth Surface Processes and Landforms.* **41**: 256–270. DOI:10.1002/esp.3853.

Goto K, Miyagi K, Imamura F. 2013. Localized tsunamigenic earthquakes inferred from preferential distribution of coastal boulders on the Ryukyu Islands, Japan. *Geology* **41**: 1139–1142. DOI:10.1130/G34823.1.

Goto K, Miyagi K, Kawana T, Takahashi J, Imamura F. 2011. Emplacement and movement of boulders by known storm waves – field evidence from the Okinawa Islands, Japan. *Marine Geology* **283**: 66–78. DOI:10.1016/j.margeo.2010.09.007.

Hansom JD, Barltrop NDP, Hall AM. 2008. Modelling the processes of cliff-top erosion and deposition under extreme storm waves. *Marine Geology* **253**: 36–50. DOI:10.1016/j.margeo.2008.02.015.

Holthuijsen LH. 2007. Waves in Oceanic and Coastal Waters. Cambridge University Press: Cambridge; 387.

Imamura F, Goto K, Ohkubo S. 2008. A numerical model for the transport of a boulder by tsunami. *Journal of Geophysical Research* **113**: C01008. DOI:10.1029/2007JC004170.

Knight J, Burningham H. 2011. Boulder dynamics on an Atlantic-facing rock coastline, northwest Ireland. *Marine Geology* **283**: 56–65. DOI:10.1016/j.margeo.2010.07.008.

Lewis M, Horsburgh K, Bates P, Smith R. 2011. Quantifying the Uncertainty in Future Coastal Flood Risk Estimates for the U.K. *Journal of Coastal Research* **27**(5): 870–881. DOI:http://dx.doi.org/10.2112/JCOASTRES-D-10-00147.1.

Lorang MS. 2011. A wave-competence approach to distinguish between boulder and megaclast deposits due to storm waves versus tsunamis. *Marine Geology* **283**: 90–97. DOI:10.1016/j.margeo.2010.10.005.

Lutz R. 2011. Metrology musings: uncertainty? There's an App for that. http://www.amrl.net/amrlsitefinity/default/Resources/newsletter/Spring2011/4.aspx [7 December 2015].

Maniatis G, Hoey T, Sventek J. 2013. Sensor enclosures: example application and implications for data coherence. *Journal of Sensor and Actuator Networks* **2**: 761–779. DOI:10.3390/jsan2040761.

Masselink G, Scott T, Poate T, Russell P, Davidson M, Conley D. 2016. The extreme 2013/2014 winter storms: hydrodynamic forcing and coastal response along the southwest coast of England. *Earth Surface Processes and Landforms.* DOI:10.1002/esp.3836.

Mastronuzzi G, Sanso P. 2004. Large boulder accumulations by extreme waves along the Adriatic coast of southern Apulia (Italy). *Quaternary International* **120**: 173–184. DOI: 10.1016/j.quaint.2004.01.016

McDonald RE. 2011. Understanding the impact of climate change on Northern Hemisphere extra-tropical cyclones. *Climate Dynamics* **37**: 1399–1425. DOI:10.1007/s00382-010-0916-x.

McNamara JP, Borden C. 2004. Observations on the movement of coarse gravel using implanted motion-sensing radio transmitters. *Hydrological Processes* **18**: 1871–1884. DOI: 10.1002/hyp.1453

Met Office. 2014. The Recent Storms and Floods in the UK. Met Office: Exeter; 27.

Mizuta R, Matsueda M, Endo H, Yukimoto S. 2011. Future change in extra-tropical cyclones associated with change in the upper troposphere. *Journal of Climate* **24**: 6456–6470.

Nandasena NAK, Paris R, Tanaka T. 2011. Reassessment of hydrodynamic equations: minimum flow velocity to initiate boulder transport by high energy events (storms, tsunamis). *Marine Geology* **281**: 70–84. DOI: 10.1016/j.margeo.2011.02.005

Nandasena NAK, Tanaka N, Sasaki Y, Osada M. 2013. Boulder transport by the 2011 Great East Japan tsunami: comprehensive field observations and whither model predictions? *Marine Geology* **346**: 292–309. DOI: 10.1016/j.margeo.2013.09.015

Naylor LA. 2001. Examining the Contribution of Biota to Rock Coast Processes, Glamorgan Heritage Coast, South Wales, Unpublished DPhil Thesis. University of Oxford.

Naylor LA, Stephenson WJ. 2010. On the role of discontinuities in mediating shore platform erosion. *Geomorphology* **114**(1-2): 89–100. DOI:10.1016/j.geomorph.2008.12.024.

Naylor LA, Coombes MA, Viles HA. 2012. Reconceptualising the role of organisms in the erosion of rock coasts: a new model. *Geomorphology* **157–158**: 17–30. DOI: 10.1016/j.geomorph.2011.07.015

Naylor LA, Kennedy DM, Stephenson WJS. 2014. Conclusions to rock coasts of the world. In Rock Coast Geomorphology: A Global Synthesis, Kennedy DM, Stephenson WJS, Naylor LA (eds). Geological Society of London Memoir Series, **40**. The Geological Society: London; chapter 17, 283–286. DOI: 10.1144/M40.17

Noormets R, Crook KAW, Felton EA. 2004. Sedimentology of rocky shorelines: 3. Hydrodynamics of megaclast emplacement and transport on a shore platform, Oahu, Hawaii. *Sedimentary Geology* **172**: 41–65. DOI: 10.1016/j.sedgeo.2004.07.006

Nott J 2003. Waves, coastal boulder deposits and the importance of the pre-transport setting. *Earth and Planetary Science Letters* **210**: 269–276. DOI:10.1016/S0012-821X(03)00104-3.

Nott J 2011. Outlook for boulder studies within tropical geomorphology and coastal hazard research. In Encyclopedia of Modern Coral Reefs Structure, Form and Process, Hopley D (ed). Springer: Dordrecht; 165–166.

Ortego MI, Tolosana-Delgado R, Gibergans-Baguena J, Egozcue JJ, Sanchez-Archilla A. 2012. Assessing wavestorm hazard evolution in the NW Mediterranean with hindcast and buoy data. *Climatic Change* **113**: 713–731. DOI: 10.1007/s10584-011-0388-y

Paris R, Naylor LA, Stephenson WJS. 2011. Boulders as a signature of storms on rock coasts. *Marine Geology* **283**: 1–11. DOI:10.1016/j.margeo.2011.03.016.

Peréz-Alberti A, Trenhaile AS. 2015. An initial evaluation of drone-based monitoring of boulder beaches in Galicia, north-western Spain. *Earth Surface Processes and Landforms* **40**: 105–111. DOI: 10.1002/esp.3654

Stephenson WJS, Naylor LA. 2011. Geological controls on boulder production in a rock coast setting: Insights from South Wales, UK. *Marine Geology* **283**: 12–24. DOI: 10.1016/j.margeo.2010.07.001

Stockdale RJ, Mclelland SJ, Middleton R, Coulthard T. 2008. Measuring river velocities using GPS River Flow Tracers (GRiFTers). *Earth Surface Processes and Landforms* **33**(8): 1315–1322. DOI: 10.1002/esp.1614

Terry JP, Lau AYA, Etienne S. 2013. Outlook for boulder studies within tropical geomorphology and coastal hazard research. In Reef-Platforms Coral Boulders, Terry JP, Etienne S, Lau AYA (eds). Springer Briefs in Earth Sciences: Dordrecht; 97–102.

Trenhaile AS. 1972. The shore platforms of the Vale of Glamorgan, Wales. *Transactions. Institute of British Geographers* **56**: 127–144. DOI:10.2307/621545.

Turton J, Fenna P. 2008. Observations of extreme wave conditions in the north-east Atlantic during December 2007. *Weather* **63**: 352–355. DOI: 10.1002/wea.321

Weiss R, Diplas P. 2015. Untangling boulder dislodgement in storms and tsunamis: is it possible with simple theories? *Geochemistry, Geophysics, Geosystems* **16**: 890–898 DOI: 10.1002/2014GC005682

Wong PP, Losada IJ, Gattuso JP, Hinkel J, Khattabi A, McInnes KL, Saito Y, Sallenger A. 2014. Coastal systems and low-lying areas. In *Climate Change 2014*: *Impacts, Adaptation, and Vulnerability. Part A*: *Global and Sectoral Aspects*, Contribution of Working Group II to the Fifth Assessment Report of the Intergovernmental Panel on Climate Change, Field CB, Barros VR, Dokken DJ, Mach KJ, Mastrandrea MD, Bilir TE, Chatterjee M, Ebi KL, Estrada YO, Genova RC, Girma B, Kissel ES, Levy AN, MacCracken S, Mastrandrea PR, White LL (eds). Cambridge University Press: Cambridge; 361–409.